Plasmon-assisted mass sensing in a hybrid nanocrystal coupled to a nanomechanical resonator

Jin-Jin Li and Ka-Di Zhu*

Key Laboratory of Artificial Structures and Quantum Control (MOE), Department of Physics, Shanghai Jiao Tong University, 800 Dong Chuan Road, Shanghai 200240, China

(Received 2 March 2011; revised manuscript received 12 May 2011; published 24 June 2011)

Surface plasmons on nanoparticles provide numerous ways to alternate and manipulate light at nanoscale dimensions, which have the potential to perfect the novel electronic and optical devices. Here, we demonstrate that plasmon-assisted mass sensing can be achieved in a hybrid nanocrystal coupled to a nanomechanical resonator. Compared with the traditional mass measurements, we use an all-optical technique rather than electrical circuitry, which may avoid the heat effect, to realize an ultrasensitive mass detection. The plasmon-assisted mass measurement proposed here may eventually enable sensitive measurement applications such as on-chip detection and analysis as well as identification of compounds.

DOI: 10.1103/PhysRevB.83.245421 PACS number(s): 42.50.Gy, 42.79.Hp, 78.47.jh, 85.35.Kt

I. INTRODUCTION

Modern nanotechnology has been successful in combining solid-state nanoparticles and biomaterials in one superstructure.[1–3] These coupled structures arise from assembling crystalline nanoparticles, nanowires, and surface plasmons (SP) into complex structures such as cavities, multilayer waveguides, and nanomechanical resonators (NRs).[4–6]

Depending on specific geometry and wavelength, surface plasmon polaritons (SPPs) on metals have some distinctive properties that enable them to confine light in a very small dimension and greatly enhance the intensity of light.[7,8] These unique features have stimulated the development of novel optical complex materials and deeper theoretical insights.[9,10] The realization of the coupling between the localized plasmon modes and the other nanostructures have led to the pursuit of plasmon hybridization.[11,12] This kind of research provides an intuitive picture for highly sensitive photodetections and also a platform for understanding the interaction between the plasmon modes and the other nanostructures, and eventually lead to innovative new devices. Recently, coupling a plasmon waveguide to a superconducting single-photon detector, Heeres *et al.*[13] have demonstrated the on-chip electrical detection of single plasmons propagating along gold waveguides.

Besides, another exciting nanostructure material is the nanomechanical resonator (NR), which is drawing interest from both technical and scientific communities in physics, chemistry, and biology because of its limited environment, high-Q factor, and small size.[14] The coupled NR systems such as NR-semiconductor quantum dot (SQD), NR-metal nanoparticle (MNP),[15,16] and the buckling nanobars[17,18] have been used to study fundamental quantum effects and high-precision measurements.

Taking advantage of these nanostructures, in the present paper, we theoretically propose a hybrid structure with a metallic nanoparticle and a semiconductor quantum dot embedded in a doubly clamped nanomechanical resonator. We show that due to the plasmon resonance, this nanocrystal complex coupled to the NR can be used as a sensitive mass detection. Previously, samples as light as 7 zeptograms ($1\ \mathrm{zg} = 10^{-21}$ g) have been weighed in vacuum by using a carbon nanotube, a nanomechanical resonator, and a fluid-filled microchannel cantilever.[19–21] During this mass sensing, even though all air can be removed from the nanomechanical resonators, they still lose energy to the electrical circuitry that is used to measure them.[22] Also, because of the heat effect, these mass detections are not suitable for the high frequency of the NR.[14,23] However, in our method, instead of electrical measurement, we use an all-optical technique to weigh small nano-objects based on a hybrid nanocrystal coupled to a nanomechanical resonator. In this way, we demonstrate a mass-detection process with surface plasmons that can be applied to the construction of sensitive sensors and efficient photocells.[24,25] The accreted mass landing on the NR can be weighed conveniently and precisely in terms of the frequency shift of the probe absorption spectrum in the presence of another strong pump laser. Most recently, the pump-probe technique proposed here has been realized by Weis *et al.*[26] in a cavity optomechanical system.

II. THEORY

The plasmon-assisted mass sensing is based on a hybrid nanocrystal consisting of a metal nanoparticle (such as Au) and a semiconductor quantum dot embedded in a doubly clamped suspended nanomechanical resonator as shown in Fig. 1. The entire system is subjected to a strong-pump beam and a weak-probe beam. At low temperature, the SQD can be modeled as a two-level system consisting of the ground state $|g\rangle$ and the first excited state $|ex\rangle$ (single exciton), and can be characterized by the pseudospin-1/2 operators $S^{\pm}$ and S^{z} (see Refs. 27 and 28). Then the Hamiltonian of this two-level exciton can be described as $H_{\mathrm{ex}} = \hbar\omega_{\mathrm{ex}} S^{z}$, where ω_{ex} is the frequency of the exciton.

Besides, a single MNP is placed above the SQD that has a radius a_0 and a center-to-center distance R from the SQD (see Fig. 1). During the extension and compression of this coupled structure, the slight shape modification of metal nanoparticle will not alter the plasmon distribution on the MNP, and then the interaction between the MNP and the NR can be neglected. The direct optical excitation of surface plasmon on MNP provides an external localized plasmon laser to this coupled SQD-NR system.[29] This plasmon laser will enhance light intensity and lead to ultrasensitive measurement. The

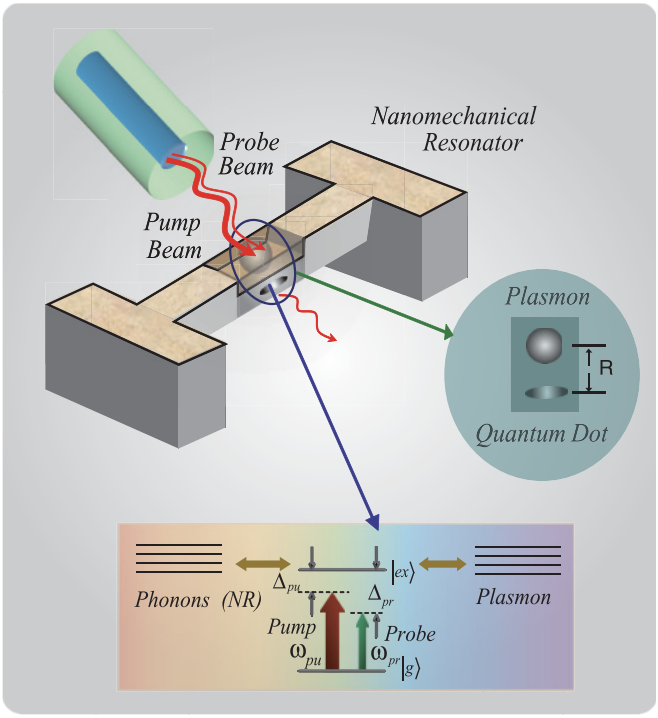

FIG. 1. (Color online) Schematic diagram of a hybrid MNP-QD complex embedded in the center of doubly clamped nanomechanical resonator. When applying two optical beams, one is strong pump beam, the other is weak probe beam, this coupled system can be used as plasmon-assisted mass spectrometry. The inset below shows the energy levels of quantum dot while dressing the plasmon field and the vibration of nanomechanical resonator.

hybrid MNP-SQD nanocrystal is embedded in the center of the nanomechanical resonator.

For the nanomechanical resonator, since the thickness is smaller than its width, the lowest-energy resonance corresponds to the fundamental flexural mode that will constitute the resonator mode. Then the Hamiltonian of this resonator is given by $H_n = \hbar\omega_n a^+ a$, where a and a^+ are the annihilation and creation operator of the resonator mode, respectively, and ω_n is the vibrational frequency of the NR. Furthermore, since the flexion induces the extension and compression in the structure of Fig. 1, the longitudinal strain will modify the energy of the electronic states of the SQD via the deformation-potential coupling.[30] Then the Hamiltonian of the nanomechanical resonator coupled to the quantum dot is described by $H_{\text{QD-}n} = \hbar\omega_n\beta S^z(a^+ + a)$, where β is the coupling strength between the NR and the SQD.

Considering the exciton in SQD interacts with a strong pump beam E_{pu} (with frequency ω_{pu}) and a weak probe beam E_{pr} (with frequency ω_{pr}), the Hamiltonian of the hybrid MNP-SQD coupled to the NR can be written as[30–33]

$$H = \hbar\omega_{\text{ex}} S^z + \hbar\omega_n a^+ a + \hbar\omega_n\beta S^z(a^+ + a) - \mu(E_{\text{SQD}} S^+ + E^*_{\text{SQD}} S^-), \quad (1)$$

where μ is the dipole element of the exciton and E_{SQD} is the total optical field felt by the SQD. In a rotating frame at the pump frequency ω_{pu}, the total Hamiltonian is given by

$$H = \hbar\Delta_{\text{pu}} S^z + \hbar\omega_n a^+ a + \hbar\omega_n\beta S^z(a^+ + a) - \mu(\tilde{E}_{\text{SQD}} S^+ + \tilde{E}^*_{\text{SQD}} S^-), \quad (2)$$

where $\Delta_{\text{pu}} = \omega_{\text{ex}} - \omega_{\text{pu}}$ is the frequency detuning between the exciton and pump field, and when the applied field is parallel (perpendicular) to the major axis of the system, we have

$$\tilde{E}_{\text{SQD}} = E_{\text{pu}} + E_{\text{pr}} e^{-i\delta t} + \frac{1}{4\pi\varepsilon_0}\frac{S_\alpha P_{\text{MNP}}}{\varepsilon_{\text{eff1}} R^3}, \quad (3)$$

$$\varepsilon_{\text{eff1}} = \frac{2\varepsilon_b + \varepsilon_s}{3\varepsilon_b}, \quad (4)$$

$$S_\alpha = 2(-1), \quad (5)$$

where $\delta = \omega_{\text{pu}} - \omega_{\text{pr}}$ is the frequency detuning of the pump and probe field, ε_0, ε_b, and ε_s are the dielectric constants of the vacuum, background medium, and SQD, respectively). Since the cross section of nanomechanical resonator is very small, the part of field emanating from the resonance MNP will lie out of the resonator, consequently the background dielectric constants should be represented by an effective dielectric constant $\varepsilon_b = (0.7\varepsilon_{\text{air}} + 0.3\varepsilon_{\text{NR}})$, where ε_{air} and ε_{NR} denote the dielectric constant of air and nanomechanical resonator (assuming that 30% of the plasmon field lies in the nanomechanical resonator[34]), respectively.

If we choose the metal nanoparticle as Au particle, the polarization of the Au MNP is

$$P_{\text{MNP}} = 4\pi\varepsilon_0\gamma a^3\left(E_{\text{pu}} + E_{\text{pr}} e^{-i\delta t} + \frac{1}{4\pi\varepsilon_0}\frac{S_\alpha P_{\text{SQD}}}{\varepsilon_{\text{eff2}} R^3}\right), \quad (6)$$

where[32,33,35]

$$\gamma = \frac{\varepsilon_{\text{Au}}(\omega) - \varepsilon_b}{2\varepsilon_b + \varepsilon_{\text{Au}}(\omega)}, \quad (7)$$

$$\varepsilon_{\text{eff2}} = \frac{2\varepsilon_b + \varepsilon_{\text{Au}}(\omega)}{3\varepsilon_b}. \quad (8)$$

The Drude model is employed for the dielectric function of gold $\varepsilon_{\text{Au}} = \varepsilon_\infty - \omega_p^2/[\omega(\omega + i\gamma_p)]$,[36] the symbols of ε_∞, ω_p, and γ_p denote, respectively, the dielectric constant of gold at large frequency, plasmon frequency, and the Drude damping constant. The dipole moment of the SQD is expressed via the off-diagonal elements of the density matrix: $P_{\text{SQD}} = \mu S^-$.[37] The dipole approximation used here is reasonable when the distance R is large and the exciton-plasmon interaction is relatively weak.[33] Therefore, the total optical field felt by the SQD is $E_{\text{SQD}} = A(E_{\text{pu}} + E_{\text{pr}} e^{-i\delta t}) + \mu B S^-$, where

$$A = 1 + \frac{\gamma a^3 S_\alpha}{\varepsilon_{\text{eff1}} R^3}, \quad (9)$$

$$B = \frac{\gamma a^3 S_\alpha^2}{\varepsilon_{\text{eff1}}\varepsilon_{\text{eff2}} R^6}. \quad (10)$$

The Heisenberg equation of motion $dO/dt = -i[O,H]/\hbar$ is employed to give the temporal evolutions of the exciton in the SQD and the nanomechanical resonator. The commutation relations $[S^z, S^\pm] = \pm S^\pm$, $[S^+, S^-] = 2S^z$, and $[a^+, a] = 1$ are used. If we set $Q = a^+ + a$, and ignore the quantum properties

of S^z, S^-, and Q, then the semiclassical equations read as follows[31]

$$\frac{d\langle S^z\rangle}{dt} = -\Gamma_1\left(\langle S^z\rangle + \frac{1}{2}\right) + i\Omega(A^*\langle S^-\rangle - A\langle S^+\rangle) + \frac{i\mu^2}{\hbar}[\langle S^+\rangle\langle S^-\rangle(B - B^*)] + \frac{i\mu}{\hbar}(A^*E_{\rm pr}^*\langle S^-\rangle e^{i\delta t} - AE_{\rm pr}\langle S^+\rangle e^{-i\delta t}), \quad (11)$$

$$\frac{d\langle S^-\rangle}{dt} = -[\Gamma_2 + i(\Delta + \omega_n\beta\langle Q\rangle)]\langle S^-\rangle - 2i\Omega A\langle S^z\rangle - \frac{2i\mu}{\hbar}AE_{\rm pr}e^{-i\delta t} - \frac{2i\mu^2\langle S^z\rangle\langle S^-\rangle}{\hbar}, \quad (12)$$

$$\frac{d^2\langle Q\rangle}{dt^2} + \gamma_n\frac{d\langle Q\rangle}{dt} + \omega_n^2\langle Q\rangle = -2\beta\omega_n^2\langle S^z\rangle, \quad (13)$$

where $\Omega = \mu E_{\rm pu}/\hbar$ is the Rabi frequency of the pump field, Γ_1 and Γ_2 denote the exciton relaxation rate and the exciton dephasing rate, respectively. Variable γ_n is the decay rate of the nanomechanical resonator due to the coupling to a reservoir of "background" modes and the other intrinsic processes.[30,38] The background will exhibit sharp resonances corresponding to the other modes. The coupling to other modes of the NR will affect the sensitivity of our mass-sensing scheme via the decay rate. If the resonances of these modes are detuned from ω_n and $2\omega_n$, the effect of the couplings on our scheme is negligible.[30,38]

In order to solve these equations, we make the following ansatz:[31]

$$S^z = S_0^z + S_1^z e^{-i\delta t} + S_{-1}^z e^{i\delta t}, \quad (14)$$

$$S^- = S_0 + S_1 e^{-i\delta t} + S_{-1} e^{i\delta t}, \quad (15)$$

$$Q = Q_0 + Q_1 e^{-i\delta t} + Q_{-1} e^{i\delta t}. \quad (16)$$

Upon substituting these equations into Eqs. (11)–(13), we can obtain the steady-state equations and finally S_1, which is related to the linear optical susceptibility as

$$\chi_{\rm eff}^{(1)}(\omega_{\rm pr}) = \frac{\mu}{\varepsilon_0 E_{\rm pr}}S_1 = \frac{\mu^2}{\varepsilon_0\hbar\Gamma_2}\chi^{(1)}(\omega_{\rm pr}) = \Sigma\chi^{(1)}(\omega_{\rm pr}), \quad (17)$$

where $\Sigma = \mu^2/(\varepsilon_0\hbar\Gamma_2)$, and the dimensionless linear susceptibility is given by

$$\chi^{(1)}(\omega_{\rm pr}) = \frac{2A^2 d w_0\left[\left(e + \Omega_0^2 A\right)(c + \delta_0) - B_0\Omega_0^2 A w_0\right] - A w_0 g(c + \delta_0)}{cg(c + \delta_0) - 2d[A^*(d - \delta_0) + 2iB_{I0}Aw_0]\left[\left(e + \Omega_0^2 A\right)(c + \delta_0) - B\Omega_0^2 A w_0\right]}, \quad (18)$$

where

$$c(\delta_0) = \Delta_{\rm pu0} - \delta_0 - \omega_{n0}\beta^2 w_0 + B_{R0}w_0 - i(1 - B_{I0}w_0), \quad (19)$$

$$d(\delta_0) = \Delta_{\rm pu0} + \delta_0 - \omega_{n0}\beta^2 w_0 + B_{R0}w_0 + i(1 - B_{I0}w_0), \quad (20)$$

$$e(\delta_0) = \frac{\Omega_0^2\omega_{n0}\beta^2 w_0\eta}{\Delta_{\rm pu0} - \omega_{n0}\beta^2 w_0 + B_{R0}w_0 - i(1 - B_{I0}w_0)}, \quad (21)$$

$$f(\delta_0) = \frac{\Omega_0^2\omega_{n0}\beta^2 w_0\eta}{\Delta_{\rm pu0} - \omega_{n0}\beta^2 w_0 + B_{R0}w_0 + i(1 - B_{I0}w_0)}, \quad (22)$$

$$g(\delta_0) = 2[A(c + \delta_0) - 2iB_{I0}Aw_0]\left[\left(f + \Omega_0^2 A\right)(d - \delta_0) - B_0^*\Omega_0^2 A w_0\right] - id(\Gamma_{10} - i\delta_0)(c + \delta_0)(d - \delta_0). \quad (23)$$

The auxiliary function $\eta(\omega_{\rm pr})$ is given by

$$\eta(\omega_{\rm pr}) = \frac{\omega_{n0}^2}{\omega_{n0}^2 - \delta_0^2 - i\gamma_{n0}\delta_0}, \quad (24)$$

where $w_0 = 2S_0^z$, $\delta_0 = \delta/\Gamma_2$, $\Omega_0 = \Omega/\Gamma_2$, $\omega_{n0}=\omega_n/\Gamma_2$, $\Delta_{\rm pu0}=\Delta_{\rm pu}/\Gamma_2$, $\Gamma_{10}=\Gamma_1/\Gamma_2$, $B_0=\mu^2 B/(\hbar\Gamma_2)$, $B_{R0}=\mathrm{Re}(B_0)$, and $B_{I0} = \mathrm{Im}(B_0)$. The population inversion (w_0) of the exciton in SQD is determined by the equation

$$(w_0 + 1)[(1 - B_{I0}w_0)^2 + (\Delta_{pu0} - \omega_{n0}\beta^2 w_0 + B_{R0}w_0)^2] + 2\Omega_0^2 A^2 w_0 = 0. \quad (25)$$

The nanomechanical resonators act as mass sensors due to their resonant-frequency sensitivity to the mass adsorbed by them. Even though the measurement techniques are rather challenging, the mass-sensing principle remains simple.[39] In our scheme, the nanomechanical resonator can be described by a harmonic oscillator with an effective mass m_n, a spring constant k, and a fundamental resonance frequency[20,30]

$$\omega_n = \sqrt{\frac{k}{m_n}}. \quad (26)$$

Mass sensing monitors the shift $\Delta\omega_n$ of ω_n induced by the adsorption onto the resonator of the molecular species selected to weigh. $\Delta\omega_n$ is related to the deposited mass m_d by[40]

$$m_d = \left(2\frac{m_n}{\omega_n}\right)\Delta\omega_n. \quad (27)$$

This is the direct relationship between the external accreted mass and the frequency shift of the nanomechanical resonator. Therefore, if we measure the frequency shift in the probe absorption spectrum exactly, then the accreted mass can be obtained accurately. Taking advantage of the localized-surface-plasmon laser, the signal of frequency shift is largely

enhanced in the probe absorption spectrum by using the pump-probe technique.

III. RESULTS AND DISCUSSIONS

In order to show the plasmon-assisted mass sensing clearly, we choose a realistic InAs SQD-Au MNP complex embedded in the center of GaAs nanomechanical resonator at an ambient temperature 4.2 K. For an InAs quantum dot,[30] the exciton relaxation rate $\Gamma_1 = 0.3$ GHz, the exciton dephasing rate $\Gamma_2 = 0.15$ GHz, and the electric dipole moment of the exciton is $\mu = 40$ D. The dielectric constants of the background medium and InAs SQD are $\varepsilon_b = 1$ and $\varepsilon_s = 6$, respectively.[32,33] The physical parameters of GaAs nanomechanical resonator are $(\omega_n, m_n, Q, \text{and } \varepsilon_{\text{NR}}) = (1.2\,\text{GHz}, 5.3 \times 10^{-15}\,\text{g}, 3 \times 10^4, \text{and } 14.55)$,[30,41] where m_n and Q are the effective mass and quality factor of the nanomechanical resonator, respectively. The decay rate of the NR is $\gamma_n = \omega_n/Q = 4.0 \times 10^{-5}$ GHz. The coupling strength between quantum dot and nanomechanical resonator is $\beta = 0.06$.[30] For the gold nanoparticle, the radius $a_0 = 2.5$ nm, $R = 16$ nm, $\varepsilon_{\text{air}} = 1$, $\varepsilon_\infty = 9.5$, $\hbar\omega_p = 8.95$ eV, and $\hbar\gamma_p = 0.069$ eV.[36]

In the following, using this coupled system of the MNP-QD and the nanomechanical resonator, we shall illustrate how to weigh the mass of accreted particles landing on the nanomechanical resonator in an all-optical domain. Figure 1 shows our proposed setup of the plasmon-assisted mass sensing in the presence of a strong pump and a weak probe laser. The inset in Fig. 1 shows the energy levels of the exciton when dressed with the surface plasmon and the vibration of nanomechanical resonator. In our pump-probe technique, we first aim a strong pump laser at this coupled system and then detect the probe absorption spectrum while the probe laser is applied. This two-laser technique has been experimentally demonstrated by Weis *et al.*[26] in a cavity optomechanical system. They also predicted that this technique can be used for on-chip optical device and ultrasensitive measurement.

A. Original frequency measurement of the nanomechanical resonator

According to Eq. (17), we first depict the probe absorption spectrum as a function of probe-exciton detuning $\Delta_{\text{pr}} = \omega_{\text{pr}} - \omega_{\text{ex}}$ with $\Delta_{\text{pu}} = 0$, as shown in Fig. 2(a). From this curve we find that there are two sharp peaks at both sides of the spectrum, which just correspond to the vibrational frequency of the nanomechanical resonator. Particularly, for our selected GaAs NR, the vibrational frequency is $\omega_n = 1.2$ GHz, then the two sharp peaks appear at ± 1.2 GHz in the probe absorption spectrum, respectively. These new features are different from the traditional atomic systems.[31] The two sharp peaks represent the resonance amplification and absorption of the vibrational mode of the NR. Including the middle feature in this absorption spectrum, these new phenomena can be interpreted by a dressed-state picture. As shown in Fig. 2(c), the uncoupled energy levels ($|g\rangle$ and $|ex\rangle$) on the left side [see part (1) of Fig. 2(c)] split into the dressed states $|g,n\rangle$, $|g,n+1\rangle$ and $|ex,n\rangle$, $|ex,n+1\rangle$ ($|n\rangle$ denotes the number states of the nanomechanical resonator). Part (2) gives the origin of the left negative sharp peak centered at $-\omega_n = -1.2$ GHz in the absorption spectrum, which signifies the electron making a transition from the lowest dressed level $|g,n\rangle$ to the highest dressed level $|ex,n+1\rangle$ by the simultaneous absorption of two pump photons and emission of a photon at $\omega_{\text{pu}} - \omega_n$. This process can amplify a wave at $\Delta_{\text{pr}} = -\omega_n$. Part (3) shows

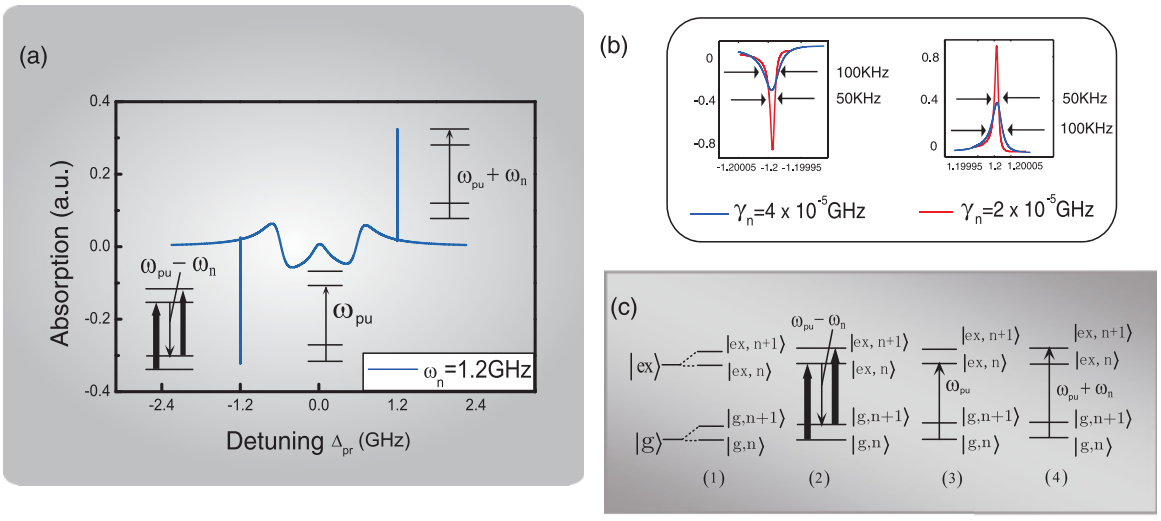

FIG. 2. (Color online) (a) The probe absorption spectrum as a function of detuning Δ_{pr} for the case $\Omega^2 = 0.05\,(\text{GHz})^2$ (corresponds to the pump intensity $I = 36\,\text{mW/cm}^2$, $\omega_n = 1.2$ GHz, $\Delta_{\text{pu}} = 0$, $\gamma_n = 4 \times 10^{-5}$ GHz, $\beta = 0.06$, $m_n = 5.3 \times 10^{-15}$ g, $a_0 = 2.5$ nm, and $R = 16$ nm). (b) The amplification of the right peak and the left peak shown in (a). The blue and the red curves for $\gamma_n = 4 \times 10^{-5}$ GHz and $\gamma_n = 2 \times 10^{-5}$ GHz have significantly different spectral widths (100 and 50 kHz). (c) The four plots are the new features shown in (a), which are identified by the corresponding transitions between the dressed states of exciton. The original two-level quantum dot can be described as the ground state and the first excited state. When dressing with the plasmon field and the vibration of NR, these two levels are split into four dressed states, which is depicted in part (1). The transitions of (2), (3), and (4) correspond to the left negative peak, the central part, and the right absorption peak shown in (a), respectively ($|n\rangle$ denotes the number states of the nanomechanical resonator).

the origin of the NR-induced stimulated Rayleigh resonance, which corresponds to a transition from the lowest dressed level $|g,n\rangle$ to the dressed level $|ex,n\rangle$. Each of these transitions is centered at the frequency of the pump laser [as shown in the middle part of Fig. 2(a)]. Furthermore, part (4) shows the right sharp peak located at $\Delta_{\rm pr} = \omega_n = 1.2$ GHz, which corresponds to the usual excitonic absorption resonance as modified by the ac-Stark effect. The underlying physical mechanism for this phenomenon can also be understood as follows. The simultaneous presence of the pump and probe fields generates a beat wave oscillating at the beat frequency $\delta = \omega_{\rm pr} - \omega_{\rm pu}$ to drive the nanomechanical resonator via the SQD. If the beat frequency δ is close to the resonance frequency ω_n of the NR, the nanomechanical resonator starts to oscillate coherently, which will result in Stokes ($\omega_s = \omega_{\rm pu} - \omega_n$) and anti-Stokes ($\omega_{\rm as} = \omega_{\rm pu} + \omega_n$) scattering of light from the pump field via the exciton in the quantum dot. For the near-resonant probe laser, the probe field will interfere with the Stokes field and the anti-Stokes field. As a result the probe spectrum can be modified significantly. Therefore, it is convenient to obtain the vibrational frequency of the nanomechanical resonator in the probe spectrum by scanning the probe frequency across the exciton frequency, provided that the pump-exciton detuning is fixed to zero. This is the key role of our plasmon-assisted mass sensing. Furthermore, Fig. 2(b) shows the dependence of the spectral width in the left peak and the right peak [shown in Fig. 2(a)] on the decay rate of the NR. The figure indicates that one can narrow the spectral width of the probe spectrum and enhance the signal of the spectrum via decreasing the decay rate of the NR. Based on this narrow spectral width (∼100 kHz), there is enough spectral resolution to do mass sensing. To obtain better sensitivity of mass sensing, we may select a smaller decay rate of the NR. It is should be noted here that the coupling to other modes of the NR will affect the sensitivity of our mass-sensing scheme via the decay rate of the NR. However, if the resonances of these modes are detuned from ω_n and $2\omega_n$, the effect of the couplings on our scheme is negligible.[30,38] In this case, the additional heating effects introduced by the coupling to the other modes are small and can also be neglected in our scheme as done for the laser cooling of the resonator.[30]

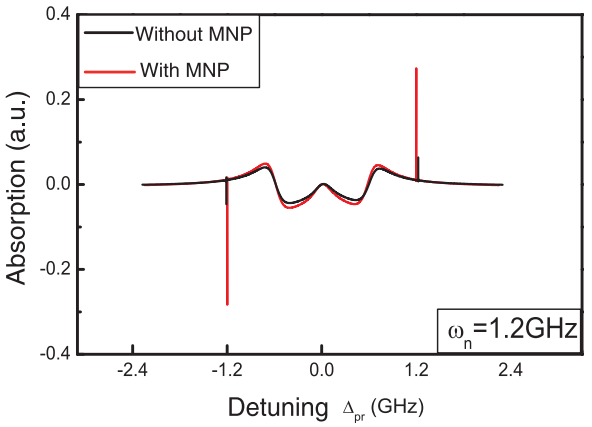

FIG. 3. (Color online) The probe absorption spectrum with and without the MNP. The other parameters are the same as in Fig. 2(a).

To illustrate the advantage of containing MNP in a coupled quantum-dot-nanomechanical-resonator system more obviously, we plot the absorption spectrum of probe laser with and without MNP as shown in Fig. 3. The red and the black curves correspond to the probe absorption with and without MNP, respectively. It is obvious that the role of MNP, in this coupled SQD-NR system, is to narrow and to enhance the probe spectrum, which will increase the sensitivity of mass sensing.

B. Mass determination

Since we have measured the frequency of nanomechanical resonator, according to Eq. (27), the next step is to determine the frequency shift while landing the deposited nanoparticle on the NR. The physical layout of the entire plasmon-assisted mass-sensing apparatus, including the nanomechanical resonator, the hybrid MNP-SQD, the evaporation system, and the

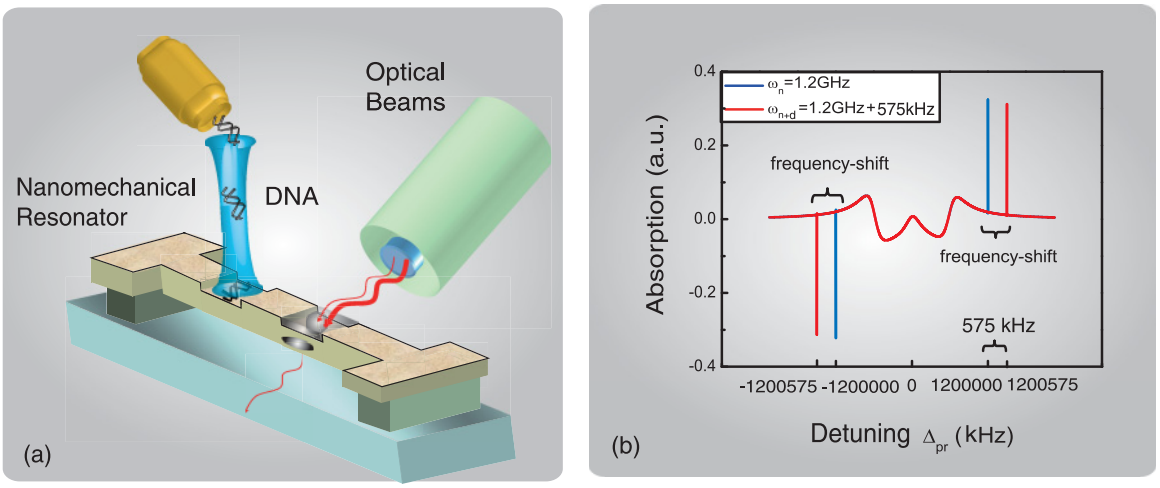

FIG. 4. (Color online) (a) The simplified process for weighing the mass of Escherichia coli strain CA46 plasmid pColG DNA with plasmon-assisted mass spectrometry. (b) The probe absorption spectrum while landing the DNA molecule on the nanomechanical resonator. The blue and the red curves are the probe absorption spectrum without and with landing DNA molecule, respectively. The other parameters are the same as in Fig. 2(a).

two optical lasers, is shown in Fig. 4(a). All the experiments are done *in situ* within a cryogenically cooled, ultrahigh vacuum apparatus with ultraslow pressure, such as below 10^{-10} Torr.

As we know, in traditional mass spectrometry, the molecules have to be ionized in the first instance and the charge on the ionized molecule needs to be known before their mass is extracted. But not all molecules are easily ionized, e.g., bioactive molecules. In this case, in order to give a guidance to experiment, we choose the landing particle as a realistic DNA molecule of the Escherichia coli strain CA46 plasmid pColG with $4715\,bp$.[42] The mass of this Escherichia coli strain plasmid is $4715 \times 2 \times 324.5/(6.022 \times 10^{23}) = 5081$ zg ($1\ \text{zg} = 10^{-21}$g). We directly put this pColG DNA upon the nanomechanical resonator in the apparatus depicted in Fig. 4(a), and then repeat the first step. We assume that the mass of DNA molecule landing on the nanomechanical resonator is uniformly distributed. Then, two new resonant peaks appear in the probe absorption spectrum that have a slight frequency shift from their original position in the first step without landing the DNA molecule. Figure 4(b) illustrates the physical picture of the frequency change. The blue curve is the original probe spectrum without landing the particle, where the two sharp peaks are located at ± 1.2 GHz, which corresponds to the inherent frequency of the nanomechanical resonator. The red curve in Fig. 4(b) is the probe absorption spectrum while landing Escherichia coli pColG DNA on the NR.

According to Eq. (27), we can absolutely determine the accreted mass m_d from the frequency shift $\Delta\omega_n$. For pColG plasmid DNA with $\Delta\omega_n = m_d\omega_n/2m_n = 575$ kHz, the new resonant steep peaks appear at $\pm 1\,200\,575$ kHz [the red curve in Fig. 4(b)]. The narrow spectral width in Fig. 2(b) provides enough spectral resolution for this mass sensing. Otherwise, the mass of multiple molecules can also be detected via landing them together onto the surface of nanomechanical resonator. It is clear that the frequency shift of the landing multiple particles is larger than that of the landing single particle.

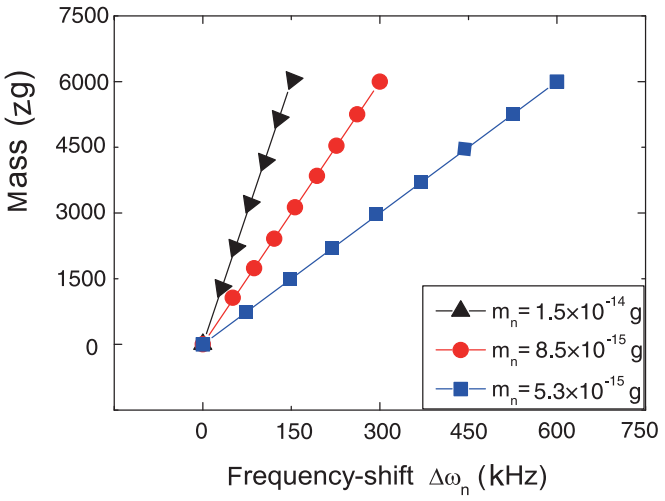

FIG. 5. (Color online) The direct proportional relationship between the accreted mass m_d and the frequency shift $\Delta\omega_n$ for different masses of the nanomechanical resonator.

C. Mass responsivity

Figure 5 displays the measurements for different nanomechanical resonators with relationship between the accreted mass and the frequency shift. The slope gives the mass responsivity of NR, i.e., $\Re = \omega_n/2m_n$, the smaller the mass of nanomechanical resonator, the higher the mass sensitivity. As discussed above, the excellent mass responsivity of the coupled SQD-NR system is attributed to both the surface plasmon of MNP and the low mass of nanomechanical resonator. Due to the advantages of surface plasmon, this plasmon-assisted mass sensing has higher sensitivity and accuracy in measuring individual molecule mass than the traditional electrical methods, which just apply to the low-frequency range (less than 1GHz) of the nanomechanical resonator.[23]

The mass responsivity is obtained assuming that all tested molecules adsorbed onto the nanomechanical resonator remain on it and also distribute uniformly along the surface of resonator. Actually, the frequency shift depends on both the mass of the arriving analyte and its position of adsorption on the nanomechanical resonator. For doubly clamped nanomechanical resonator, the observed frequency shift is maximized when the particle adsorbs at the center of the resonator. Minimal shifts are induced for adsorption near the clamping points. This result can be carried out by building a histogram of event probability versus frequency-shift amplitude for small ensembles of sequential single-molecule or single-nanoparticle adsorption events.[39]

As compared with traditional electrical methods, the main benefits of our proposed all-optical mass sensing are listed as follows: (1) operating at high frequencies, (2) avoiding the heating effect or energy loss caused by circuits, and (3) narrowing spectral width due to surface plasmons. Particularly, the spectral width of the probe spectrum in our technique is of the order of magnitude of kHz while the electric methods in Refs. 39 and 43 gave a spectral width of the order of magnitude of MHz. In this case, our proposed mass sensing based on hybrid NMP-SQD-NR system has better sensitivity than traditional electrical methods.

IV. CONCLUSIONS

In summary, we have proposed a scheme of a plasmon-assisted mass spectrometry based on a hybrid MNP-SQD system coupled to a nanomechanical resonator in all-optical domains. The accreted mass landing on the nanomechanical resonator can be measured conveniently and precisely according to the frequency shift in the probe absorption spectrum. Most notably, due to the participation of the surface plasmon, this mass sensor becomes more accurate for measuring the frequency of the resonator. According to the simple and all-optical measurement, the plasmon-assisted mass sensor proposed here has significant advantages over the traditional electrical approaches for measuring the inertial mass of particles and organic molecules including DNA molecules and proteins. Finally, we hope that our proposed device can be realized by current experiments in the near future.

ACKNOWLEDGMENTS

The part of this work has been supported by National Natural Science Foundation of China (Nos.10774101 and 10974133) and the National Ministry of Education Program for Ph.D.

*zhukadi@sjtu.edu.cn

[1] Q. Yao, L. D. Chen, W. Q. Zhang, C. Sheng, F. Liu, and X. H. Chen, ACS Nano **4**, 2445 (2010).
[2] A. D. Aguilar, E. S. Forzani, M. Leright, F. Tsow, A. Cagan, R. A. Iglesias, L. A. Nagahara, I. Amlani, R. Tsui, and N. J. Tao, Nano Lett. **10**, 380 (2010).
[3] W. H. Liu, M. Lee, L. Ding, J. Liu, and Z. L. Wang, Nano Lett. **10**, 3084 (2010).
[4] S. Balci, A. Kocabas, C. Kocabas, and A. Aydinli, Appl. Phys. Lett. **97**, 131103 (2010).
[5] K. Wang, Z. Zheng, Y. Su, Y. Wang, Z. Wang, L. Song, J. Diamond, and J. Zhu, Sensor Lett. **8**, 370 (2010).
[6] S. W. Hwang, D. H. Shin, C. O. Kim, S. H. Hong, M. C. Kim, J. Kim, K. Y. Lim, S. Kim, S. H. Choi, K. J. Ahn, G. Kim, S. H. Sim, and B. H. Hong, Phys. Rev. Lett. **105**, 127403 (2010).
[7] X. Shan, U. Patel, S. Wang, R. Iglesias, and N. Tao, Science **327**, 1363 (2010).
[8] H. Chen, T. Ming, L. Zhao, F. Wang, L.-D. Sun, J. Wang, and C.-H. Yan, Nano Today **5**, 494 (2010).
[9] Y. Liu, T. Zentgraf, G. Bartal, and X. Zhang, Nano Lett. **10**, 1991 (2010).
[10] E. Hwang, I. I. Smolyaninov, and C. C. Davis, Nano Lett. **10**, 813 (2010).
[11] N. J. Halas, Nano Lett. **10**, 3816 (2010).
[12] M. Ishifuji, M. Mitsuishi, and T. Miyashita, J. Am. Chem. Soc. **131**, 4418 (2009).
[13] R. W. Heeres, S. N. Dorenbos, B. Koene, G. S. Solomon, L. P. Kouwenhoven, and V. Zwiller, Nano Lett. **10**, 661 (2010).
[14] K. L. Ekinci and M. L. Roukes, Rev. Sci. Instrum. **76**, 061101 (2005).
[15] N. Lambert and F. Nori, Phys. Rev. B **78**, 214302 (2008).
[16] A. V. Moskalenko, S. N. Gordeev, O. F. Koentjoro, P. R. Raithby, R. W. French, F. Marken, and S. E. Savel'ev, Phys. Rev. B **79**, 241403 (2009).
[17] S. Savel'ev, A. L. Rakhmanov, X. Hu, A. Kasumov, and F. Nori, Phys. Rev. B **75**, 165417 (2007).
[18] S. Savel'ev, X. Hu, and F. Nori, New J. Phys. **8**, 105 (2006).
[19] H. Y. Chiu, P. Hung, H. W. Ch. Postma, and M. Bockrath, Nano Lett. **8**, 4342 (2008).
[20] B. Lassagne, D. Garcia-Sanchez, A. Aguasca, and A. Bachtold, Nano Lett. **8**, 3735 (2008).
[21] Y. T. Yang, C. Callegari, X. L. Feng, K. L. Ekinci, and M. L. Roukes, Nano Lett. **6**, 583 (2006).
[22] P. Skyba, J. Low Temp. Phys. **160**, 219 (2010).
[23] K. C. Schwab and M. L. Roukes, Phys. Today **58**, 36 (2005).
[24] S. N. Kim, J. M. Slocik, and R. R. Naik, Small **6**, 1992 (2010).
[25] S. Yodyingyong, Q. Zhang, K. Park, C. S. Dandeneau, X. Zhou, D. Triampo, and G. Cao, Appl. Phys. Lett. **96**, 073115 (2010).
[26] S. Weis, R. Rivière, S. Deléglise, E. Gavartin, O. Arcizet, A. Schliesser, and T. J. Kippenberg, Science **10**, 1520 (2010).
[27] A. Zrenner, E. Beham, S. Stufler, E. Findeis, M. Bichler, and G. Abstreiter, Nature (London) **418**, 612 (2002).
[28] S. Stufler, P. Ester, A. Zrenner, and M. Bichler, Phys. Rev. B **72**, 121301 (2005).
[29] R. F. Oulton, V. J. Sorger, T. Zentgraf, R. N. Ma, C. Gladden, L. Dai, G. Bartal, and X. Zhang, Nature (London) **461**, 629 (2009).
[30] I. Wilson-Rae, P. Zoller, and A. Imamoğlu, Phys. Rev. Lett. **92**, 075507 (2004).
[31] R. W. Boyd, *Nonlinear Optics* (Academic Press, Amsterdam, 2008) pp. 313.
[32] W. Zhang, A. O. Govorov, and G. W. Bryant, Phys. Rev. Lett. **97**, 146804 (2006).
[33] J. Y. Yan, W. Zhang, S. Duan, X. G. Zhao, and A. O. Govorov, Phys. Rev. B **77**, 165301 (2008).
[34] J. S. Bitten, L. A. Sweatlock, H. Mertens, N. S. Lewis, A. Polman, and H. A. Atwater, J. Phys. Chem. C **111**, 13372 (2007).
[35] R. D. Artuso and G. W. Bryant, Nano Lett. **8**, 2106 (2008).
[36] W. H. Ni, T. Ambjörnsson, S. P. Apell, H. J. Chen, and J. F. Wang, Nano Lett. **10**, 77 (2010).
[37] A. Yariv, *Quantum Electronics* (Wiley, New York, 1975).
[38] I. Wilson-Rae, Phys. Rev. B **77**, 245418 (2008).
[39] A. K. Naik, M. S. Hanay, W. K. Hiebert, X. L. Feng, and M. L. Roukes, Nat. Nanotechnol. **4**, 445 (2009).
[40] K. L. Ekinci, Y. T. Yang, and M. L. Roukes, J. Appl. Phys. **95**, 2682 (2004).
[41] O. G. Lorimor and W. G. Spitzer, J. Appl. Phys. **36**, 1841 (1965).
[42] NCBI [http://www.ncbi.nlm.nih.gov/nuccore/NC_010904].
[43] H. Y. Chiu, P. Hung, H. W. Ch. Postma, and M. Bockrath, Nano Lett. **8**, 4342 (2008).